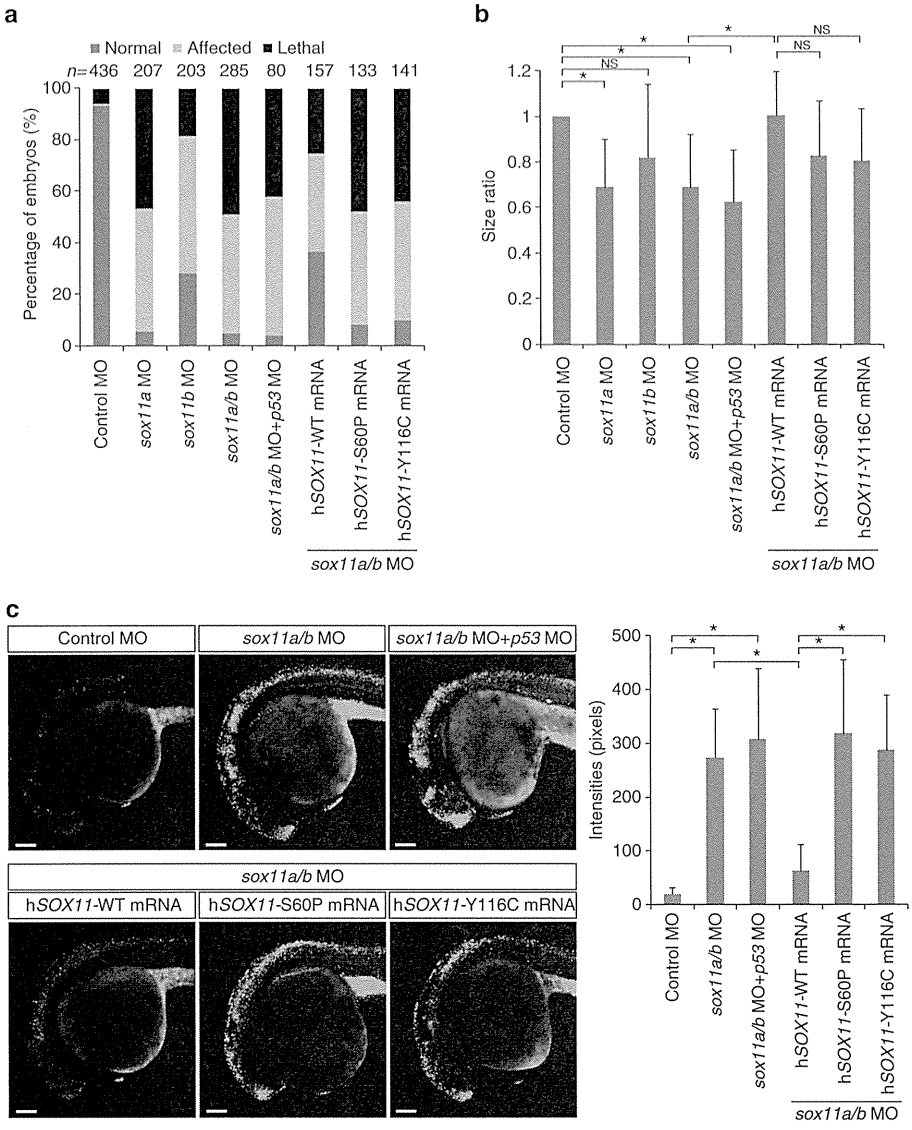

Figure 4 | *sox11a/b* knockdown experiments in zebrafish. (**a**) Embryos were injected with *sox11*-MO alone or with *sox11*- and *tp53*-MO or with *sox11*-MO and *in vitro* transcribed human *SOX11* (h*SOX11*) mRNA (WT, wild type; S60P, p.Ser60Pro; Y116C, p.Tyr116Cys). Injected embryos were categorized as normal, affected and lethal at 48 hpf. The lethal and affected phenotype in *sox11a/b*-MO-injected embryos was partially rescued by WT h*SOX11* mRNA overexpression. All experiments were performed more than twice and evaluated statistically with a Student's *t*-test. (**b**) Head size ratios of embryos with control-, *sox11a*-, *sox11b*- or *sox11a/b*-MO alone, or with *sox11a/b*- and *tp53*-MO or *sox11a/b*-MO and h*SOX11* mRNA (WT or mutant) at 48 hpf ($n \geq 10$) (average of control-MO as 1). Dorsal views of midbrain width were measured. Data are represented as mean ± s.d. $^*P < 0.05$ by Student's *t*-test. NS, not significant. (**c**) Brain cell death in MO-injected embryos at 30 hpf using acridine orange staining (lateral view). *sox11* morphants show increased cell death in the CNS. Scale bar, 100 μm. Quantification of acridine orange intensities in morphants are shown graphically (right, $n \geq 10$). Data are represented as mean ± s.d. $^*P < 0.001$ by Student's *t*-test.

In conclusion, mutations in both BAF complex genes and *SOX11* result in the same phenotype (CSS), providing strong support for the BAF complex and SOX11 function in a common pathway, and play an important role in human brain development.

Methods

Subjects and clinical data. Patients were seen by their attending clinical geneticists. DNA samples were isolated from peripheral blood leukocytes using standard methods. Informed consent was obtained from the parents of the patients for experimental protocols and displaying participants' facial appearances in publications. This study was approved by the institutional review board of Yokohama City University School of Medicine. A total of 92 patients were analysed, including 71 patients from a previous cohort and 21 new patients.

WES. Trio-based WES was performed in two families. Briefly, 3 μg of genomic DNA was sheared using the Covaris 2S system (Covaris, Woburn, MA) and partitioned using SureSelect Human All Exon V4 or V4 + UTRs (Agilent Technology, Santa Clara, CA), according to the manufacturer's instructions. Exon-enriched DNA libraries were sequenced using HiSeq2000 (Illumina, San Diego, CA) with 101-bp paired-end reads and 7-bp index reads. Four samples (2.5 pM each, with different indexes) were run in one lane. Image analysis and base calling were performed using HiSeq Control Software/Real-Time Analysis and CASAVA1.8.2 (Illumina). Mapping to human genome hg19 was performed using Novoalign (http://www.novocraft.com/main/page.php?s=novoalign). Aligned reads were

processed by Picard (http://picard.sourceforge.net) to remove PCR duplicates. Variants were called using the Genome Analysis Toolkit 1.5–21 (GATK v3) with best practice variant detection (http://gatkforums.broadinstitute.org/discussion/15/best-practice-variant-detection-with-the-gatk-v1-x-retired), and annotated by Annovar (23 February 2012) (http://www.openbioinformatics.org/annovar/). Common variants registered in dbSNP137 (MAF≥0.01) (http://genome.ucsc.edu/cgi-bin/hgTrackUi?hgsid=281702941&c=chr1&g=snp137Flagged) were removed.

Prioritization of variants. From all the variants within exons and ±2 bp of intronic regions from exon–intron boundaries, those registered in either dbSNP137, 1,000 Genomes (http://www.1000genomes.org/), ESP 6500 (http://evs.gs.washington.edu/EVS/) or our in-house (exome data from 408 individuals) databases, and those located within segmental duplications, were removed and we focused on heterozygous non-synonymous and splice site variants, which were subsequently confirmed by Sanger sequencing. *SOX11* mutations in LOVD, http://www.LOVD.nl/SOX11.

Structural modelling and free energy calculations. The crystal structure of the mouse Sox4 HMG domain bound to DNA (Protein Data Bank code 3U2B) was selected by SWISS-MODEL server 5 (ref. 25) as the structure most resembling human SOX11. To examine the missense mutations, mutational free energy changes were calculated using FoldX software (version 3.0)[10,11]. Calculations were repeated three times, and resultant data presented as average values with s.d.

***SOX11* expression analysis in human tissues.** TaqMan quantitative real-time PCR was performed using cDNAs from adult (Human MTC Panel I, #636742, Clontech Laboratories, Mountain View, CA) and foetus (Human Fetal MTC Panel, #636747, Clontech Laboratories). Pre-designed TaqMan probes for human *SOX11* (Hs00167060_m1, Life Technologies Co., Carlsbad, CA) and human beta-actin (ACTB, 4326315E, Life Technologies Co.) were used. PCR was performed on a Rotor-Gene Q (QIAGEN, Valencia, CA) and expression levels normalized to *ACTB*, an internal standard gene, according to the $2^{-\Delta\Delta Ct}$ method. Kidney expression was used as the standard (1×).

Expression vectors. The *SOX11* open-reading frame clone was purchased from Promega (Tokyo, Japan) and *SOX11* mutants (c.178T>C; p.Ser60Pro and c.347A>G; p.Tyr116Cys) generated by site-directed mutagenesis with the KOD-Plus-Mutagenesis Kit (TOYOBO, Osaka, Japan). WT and mutant *SOX11* cDNAs were PCR amplified and cloned into the pEF6/V5-His B mammalian expression vector (Life Technologies) using the In-Fusion PCR Cloning Kit (Clontech Laboratories), and also into the p3xFLAG-CMV-14 mammalian expression vector (Sigma, St Louis, MO). The *GDF5* promoter 5′-flanking sequence (−448/+319) was PCR amplified and cloned into the pGL3-basic vector (Promega). All constructs were verified by Sanger sequencing. Human *SOX11* cDNA can be obtained from GenBank/EMBL/DDBJ nucleotide core database under the accession code AB028641.1.

Immunostaining. Mouse neuroblastoma 2A (Neuro-2A) cells were cultured in Dulbecco's modified Eagle's medium (DMEM)–high glucose GlutaMAX supplemented with 10% fetal bovine serum (FBS) and penicillin-streptomycin (Life Technologies Co.). Neuro-2A cells were plated into 24-well plates, 24 h before transfection. Each expression construct (200 ng) was transfected into Neuro-2A cells using X-tremeGENE 9 DNA Transfection Reagent (Roche Diagnostics, Indianapolis, IN). Twenty-four hours after transfection, cells were fixed in 4% paraformaldehyde (PFA)/phosphate-buffered saline (PBS) for 15 min at room temperature, and permeabilized in 0.1% Triton X-100/PBS for 5 min at room temperature. C-terminal V5-6xHis-tagged SOX11 proteins were detected using a mouse anti-V5 primary antibody (1:200; Life Technologies Co.) and an Alexa Fluor 546 Goat Anti-Mouse IgG secondary antibody (1:1,000; Life Technologies Co.). Smears were mounted in Vectashield mounting medium with DAPI (Vector Lab., Burlingame, CA). Confocal images were acquired using a Fluoview FV1000-D microscope (Olympus, Tokyo, Japan).

Luciferase assay. HeLa cells were cultured in DMEM-high glucose supplemented with penicillin (50 units ml^{-1}), streptomycin (50 μg ml^{-1}) and 10% FBS. ATDC5 cells were cultured in DMEM/Ham's F-12 (1:1) supplemented with the above antibiotics and 5% FBS. Cells were plated in 24-well plates, 24 h before transfection, and transfections performed using TransIT-LT1 (Takara, Ohtsu, Japan) with pGL3 reporter (500 ng per well), effector (250 ng per well) and pRL-SV40 internal control (6 ng per well) vectors. Twenty-four hours after transfection, cells were harvested and luciferase activities measured using the PicaGene Dual SeaPansy Luminescence Kit (TOYO B-Net, Tokyo, Japan). Production of WT and mutant SOX11 proteins was assessed by immunoblot analysis with monoclonal anti-FLAG M2 HRP antibody (1:3,000; Sigma), following the manufacturer's instructions.

Morpholino and mRNA microinjection. Antisense translation-blocking morpholinos (MOs) for *sox11a*—(5′-CGCTGTTGTCCGTTTGCTGCACCAT-3′), *sox11b*—(5′-CTGTGCTCCGTCTGCTGCACCATGT-3′)[17], *tp53*—(5′-GCGCCATTGCTTTGCAAGAATTG-3′)[18] and standard control—(5′-CCTCTTACCTCAGTTACAATTTATA-3′) MO were obtained from GeneTools (Philomath, OR) and injected (or co-injected) into one- to two-cell-stage embryos at a final concentration of 0.1 or 0.2 mM. In rescue assays, capped human *SOX11* mRNAs transcribed *in vitro* from pEF6/V5-His B constructs were prepared using the mMessage mMachine T7 ULTRA Transcription Kit (Ambion, Carlsbad, CA), following the manufacturer's instructions, and injected into one-cell-stage embryos. For each MO knockdown and rescue experiment, embryos from the same clutch were used as experimental subjects and controls. Approximately 1 μg of capped RNA was injected per embryo. The experiment was authorized by the institutional committee of fish experiments in the National Research Institute of Fisheries Science.

Cell death detection. To detect apoptotic cells in live embryos, embryos at 30 hpf were manually dechorionated and incubated in acridine orange (2 μg ml^{-1} in egg water) at 28 °C for 1 h. After washing with egg water six times for 10 min each, embryos were anaesthetized with tricaine, mounted in 2% methylcellulose and examined by confocal microscopy. Apoptotic cells were also examined by the TUNEL assay, as previously described[26]. Embryos at 30 hpf, were fixed overnight in 4% PFA with PBS at 4 °C and stored in 100% methanol at −20 °C. Samples were incubated in 100% acetone at −20 °C for 20 min. Following fixation, the embryos were rinsed three times with PBS containing 0.1% Tween-20. Samples were then permeabilized by treatment with 0.5% Triton X-100 and 0.1% sodium citrate in PBS for 15 min. Embryos were subjected to the TUNEL assay by using the ApopTag Red *in situ* Apoptosis Detection Kit (Merck KGaA Millipore, Darmstadt, Germany) according to the manufacture's instruction.

Detection and quantitation of visible and fluorescent images. All animals were photographed under the same conditions using a LSM510 confocal microscope (Carl Zeiss, Jena, Germany). In each animal, acridine orange-positive cells were quantitated using a selection tool in Adobe Photoshop, for a colour range chosen by green colour selection of regions showing visually positive acridine orange staining. For analysis of embryos, defined head regions were selected in each embryo. Following pixel selection, a fuzziness setting of 0 was used, and chosen pixel numbers calculated using the image histogram calculation.

Whole-mount immunohistochemistry. For HuC/D staining, embryos at 48 hpf were fixed in 4% PFA overnight at 4 °C and dehydrated in methanol at −20 °C. For acetylated tubulin staining, embryos at 48 hpf were fixed in Dent's fixative (80% methanol and 20% dimethyl sulphoxide) overnight at 4 °C. Embryos were permeabilized with proteinase K followed by postfixation with 4% PFA and washed with PBSTX (PBS containing 0.5% Triton X-100). After treating with 4% normal goat serum (NGS) in PBSTX for 2 h at room temperature, embryos were incubated with mouse anti-HuC/D (1:500, A21271, Life Technologies Co.) or mouse anti-acetylated tubulin (1:1,000, T7451, Sigma) antibodies in 4% NGS/PBSTX overnight at 4 °C. Embryos were washed five times with PBSTX for 10 min each and incubated with goat anti-mouse fluorescein isothiocyanate secondary antibody diluted in 2% NGS/PBSTX for 2 h at room temperature. After washing five times for 10 min each, embryos were mounted in 2% methylcellulose and examined using a Fluoview FV1000-D confocal microscope (Olympus).

References

1. Ronan, J. L., Wu, W. & Crabtree, G. R. From neural development to cognition: unexpected roles for chromatin. *Nat. Rev. Genet.* **14,** 347–359 (2013).
2. Tsurusaki, Y. *et al.* Mutations affecting components of the SWI/SNF complex cause Coffin-Siris syndrome. *Nat. Genet.* **44,** 376–378 (2012).
3. Tsurusaki, Y. *et al.* Coffin-Siris syndrome is a SWI/SNF complex disorder. *Clin. Genet.* **85,** 548–554 (2014).
4. Santen, G. W. E. *et al.* Mutations in SWI/SNF chromatin remodeling complex gene ARID1B cause Coffin-Siris syndrome. *Nat. Genet.* **44,** 379–380 (2012).
5. Santen, G. W. E. *et al.* Coffin-Siris syndrome and the BAF complex: genotype-phenotype study in 63 patients. *Hum. Mutat.* **34,** 1519–1528 (2013).
6. Wieczorek, D. *et al.* A comprehensive molecular study on Coffin-Siris and Nicolaides-Baraitser syndromes identifies a broad molecular and clinical spectrum converging on altered chromatin remodeling. *Hum. Mol. Genet.* **22,** 5121–5135 (2013).
7. Van Houdt, J. K. *et al.* Heterozygous missense mutations in SMARCA2 cause Nicolaides-Baraitser syndrome. *Nat. Genet.* **44,** 445–449 (2012).
8. Kosho, T. *et al.* Clinical correlations of mutations affecting six components of the SWI/SNF complex: detailed description of 21 patients and a review of the literature. *Am. J. Med. Genet. A* **161,** 1221–1237 (2013).
9. Jauch, R., Ng, C. K., Narasimhan, K. & Kolatkar, P. R. The crystal structure of the Sox4 HMG domain-DNA complex suggests a mechanism for positional interdependence in DNA recognition. *Biochem. J.* **443,** 39–47 (2012).
10. Guerois, R., Nielsen, J. E. & Serrano, L. Predicting changes in the stability of proteins and protein complexes: a study of more than 1000 mutations. *J. Mol. Biol.* **320,** 369–387 (2002).

11. Schymkowitz, J. *et al.* The FoldX web server: an online force field. *Nucleic Acids Res.* **33,** W382–W388 (2005).
12. Khan, S. & Vihinen, M. Performance of protein stability predictors. *Hum. Mutat.* **31,** 675–684 (2010).
13. Kan, A. *et al.* SOX11 contributes to the regulation of GDF5 in joint maintenance. *BMC Dev. Biol.* **13,** 4 (2013).
14. Sock, E. *et al.* Gene targeting reveals a widespread role for the high-mobility-group transcription factor Sox11 in tissue remodeling. *Mol. Cell. Biol.* **24,** 6635–6644 (2004).
15. Rimini, R. *et al.* Expression patterns of zebrafish sox11A, sox11B and sox21. *Mech. Dev.* **89,** 167–171 (1999).
16. de Martino, S. *et al.* Expression of sox11 gene duplicates in zebrafish suggests the reciprocal loss of ancestral gene expression patterns in development. *Dev. Dyn.* **217,** 279–292 (2000).
17. Gadi, J. *et al.* The transcription factor protein sox11 enhances early osteoblast differentiation by facilitating proliferation and the survival of mesenchymal and osteoblast progenitors. *J. Biol. Chem.* **288,** 25400–25413 (2013).
18. Robu, M. E. *et al.* p53 activation by knockdown technologies. *PLoS Genet.* **3,** e78 (2007).
19. Berghmans, S. *et al.* tp53 mutant zebrafish develop malignant peripheral nerve sheath tumors. *Proc. Natl Acad. Sci. USA* **102,** 407–412 (2005).
20. Sarkar, A. & Hochedlinger, K. The sox family of transcription factors: versatile regulators of stem and progenitor cell fate. *Cell Stem Cell* **12,** 15–30 (2013).
21. Fantes, J. *et al.* Mutations in SOX2 cause anophthalmia. *Nat. Genet.* **33,** 461–463 (2003).
22. Pingault, V. *et al.* SOX10 mutations in patients with Waardenburg-Hirschsprung disease. *Nat. Genet.* **18,** 171–173 (1998).
23. Wagner, T. *et al.* Autosomal sex reversal and campomelic dysplasia are caused by mutations in and around the SRY-related gene SOX9. *Cell* **79,** 1111–1120 (1994).
24. Ninkovic, J. *et al.* The BAF complex interacts with Pax6 in adult neural progenitors to establish a neurogenic cross-regulatory transcriptional network. *Cell Stem Cell* **13,** 403–418 (2013).
25. Kiefer, F., Arnold, K., Kunzli, M., Bordoli, L. & Schwede, T. The SWISS-MODEL Repository and associated resources. *Nucleic Acids Res.* **37,** D387–D392 (2009).
26. Koshimizu, E. *et al.* Embryonic senescence and laminopathies in a progeroid zebrafish model. *PLoS ONE* **6,** e17688 (2011).

Acknowledgements

We thank the individuals and their families for participation in this study. We also thank Nobuko Watanabe for her technical assistance. This work was supported by the Ministry of Health, Labour and Welfare of Japan; the Japan Society for the Promotion of Science (a Grant-in-Aid for Scientific Research (B), and a Grant-in-Aid for Scientific Research (A)); the Takeda Science Foundation; the fund for Creation of Innovation Centers for Advanced Interdisciplinary Research Areas Program in the Project for Developing Innovation Systems; the Strategic Research Program for Brain Sciences; and a Grant-in-Aid for Scientific Research on Innovative Areas (Transcription Cycle) from the Ministry of Education, Culture, Sports, Science and Technology of Japan. The Indian Council of Medical Research, New Delhi is also appreciated for funding support for the DNA banking facility.

Author contributions

Y.T. and N.Ma. designed and directed the study. Y.T., E.K. and N.Ma. wrote the manuscript. H.O. and S.P. collected samples and provided subjects' clinical information. N.O. evaluated clinical information. Y.T., T.S., S.M., M.N., H.S., S.W., K.-i.Y. and N.Mi. performed exome and Sanger sequencing. E.K., S.Ima. and M.Y. performed zebrafish experiments. I.K. and S.Ike. performed luciferase assays. M.S. and K.O. performed crystal structural analysis. Y.T. and H.K. analysed protein localization.

Additional information

Accession codes: Exome sequence data for CSS patients have been deposited in the Human Genetic Variation Browser under the accession code HGV0000001 (http://www.genome.med.kyoto-u.ac.jp/SnpDB/repository/HGV0000001.html). Access to this data is controlled by the Yokohama City University Data Access Committee.

Supplementary Information accompanies this paper at http://www.nature.com/naturecommunications

Competing financial interests: The authors declare no competing financial interests.

Reprints and permission information is available online at http://npg.nature.com/reprintsandpermissions/

How to cite this article: Tsurusaki, Y. *et al. De novo SOX11* mutations cause Coffin–Siris syndrome. *Nat. Commun.* 5:4011 doi: 10.1038/ncomms5011 (2014).

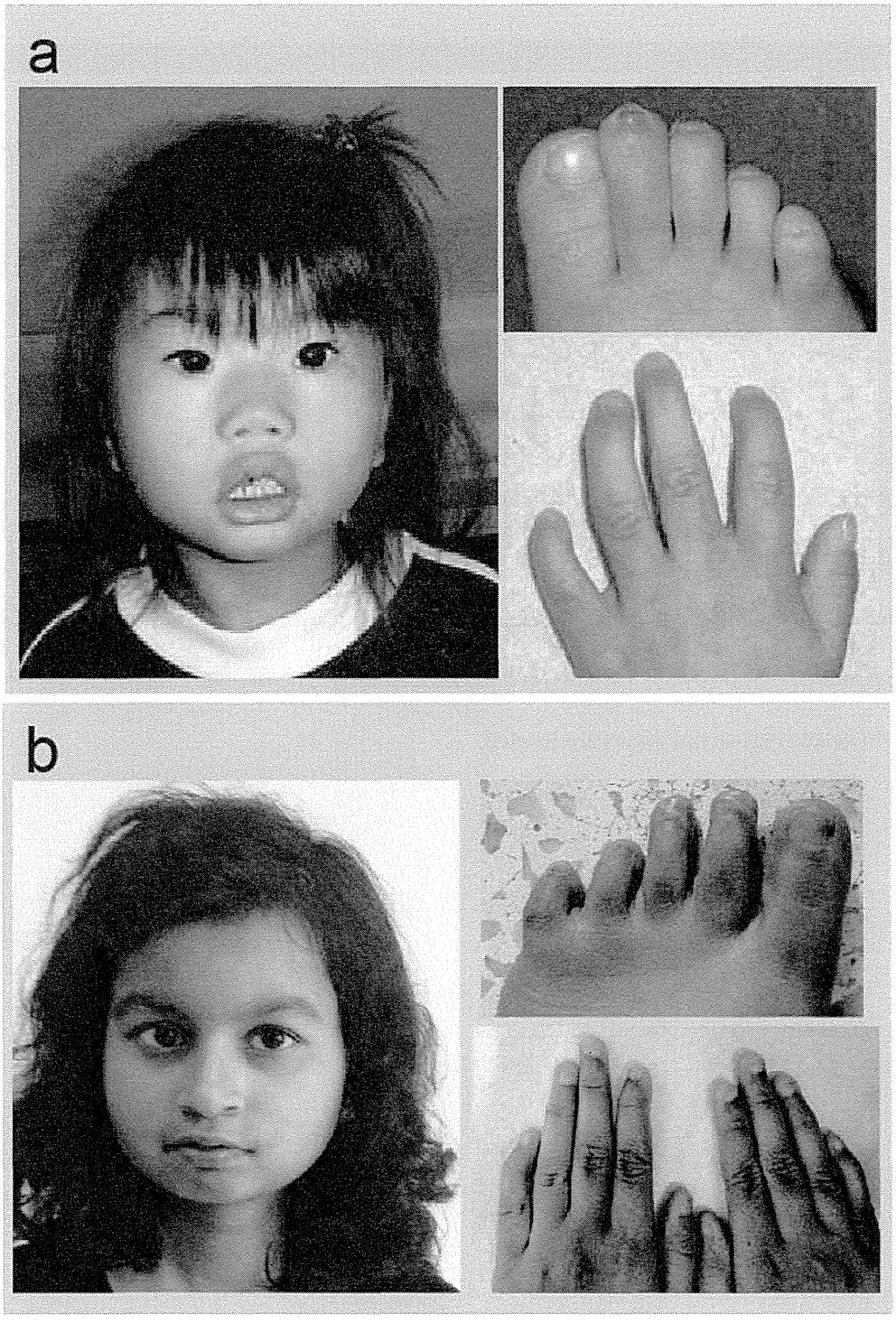

Supplementary Figure 1. Clinical features of CSS patients with *SOX11* mutations.

Photographs of face, right foot and left hand of Patient 1 at 5 years (**a**), and Patient 2 at 16 years (**b**). Arched eyebrows, low set ears and nail hypoplasia are observed in common.

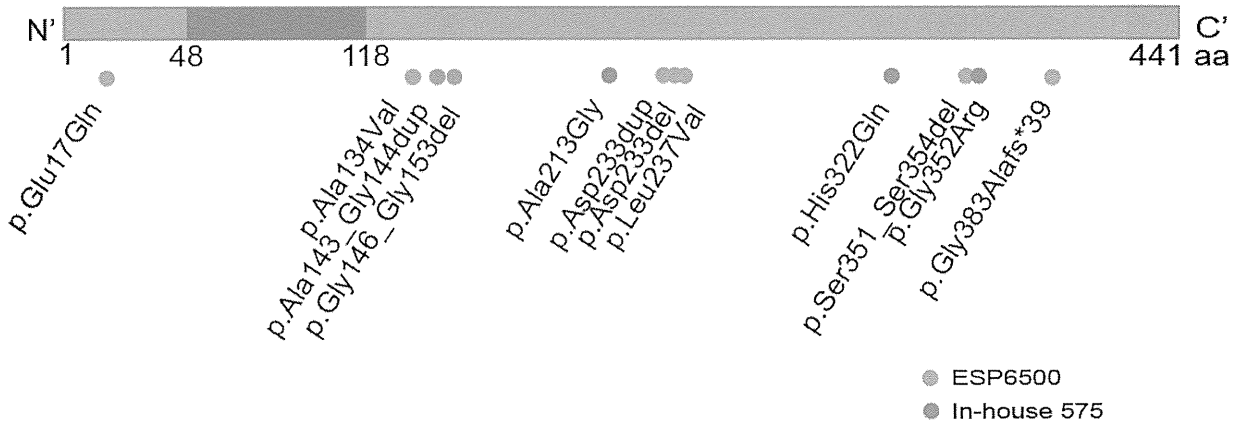

Supplementary Figure 2. Database identification of *SOX11* variants.

A total of 22 *SOX11* variants were found in the databases examined (ESP6500, 1000 Genomes and our in-house databases containing 575 control exomes) (Supplementary Table 1). Among these, missense and indel variants, but not synonymous variants, are depicted as dots. The blue box indicates the HMG domain where the two heterozygous mutations are located.

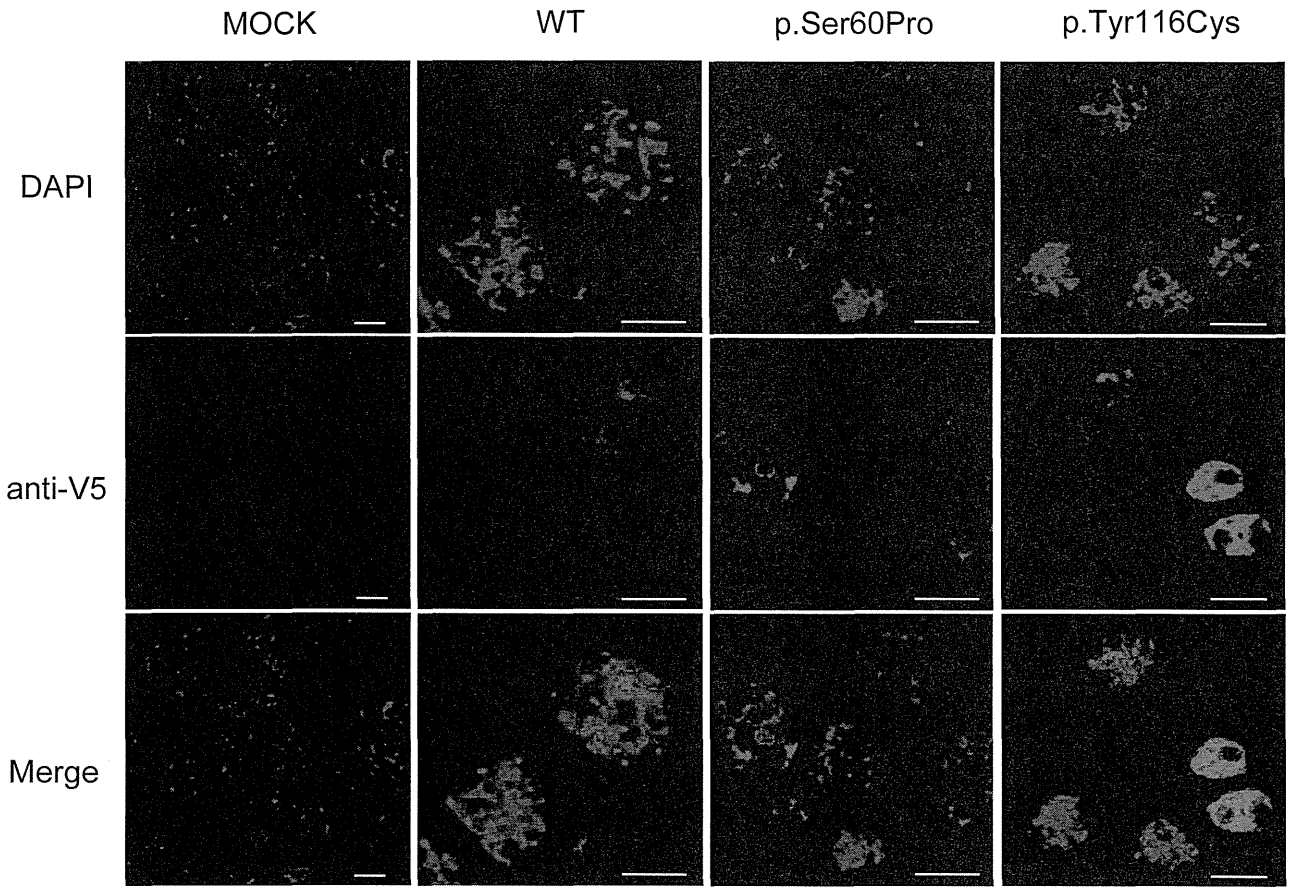

Supplementary Figure 3. SOX11 protein localization.

Immunostaining of Neuro-2A cells transfected with expression vectors containing C-terminal V5-6xHis-tagged WT (2nd column) and mutant SOX11, p.Ser60Pro (3rd column) and p.Tyr116Cys (4th column). SOX11 protein was detected using an anti-v5 antibody coupled to Alexa Fluor 488 as the secondary antibody (red). Nuclei were stained with DAPI (blue). Similar to WT protein, nuclear localization of mutant proteins is observed. Scale bar=10 μm.

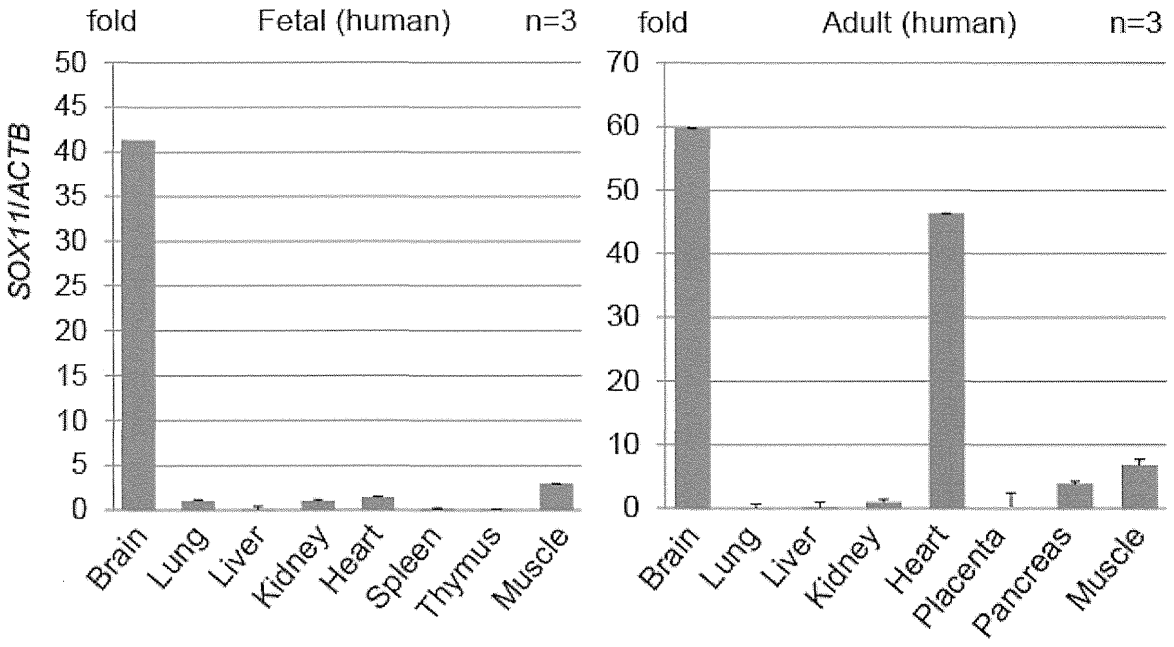

Supplementary Figure 4. *SOX11* expression in human tissues.

SOX11 expression determined using TaqMan quantitative real-time PCR assay of human adult (right) and fetal (left) tissue cDNAs. Error bars represent standard deviations of three independent experiments. Kidney expression was used as the expression standard (1x). Muscle indicates skeletal muscle. Brain specific expression in fetus and adult, as well as high heart expression in adult was detected.

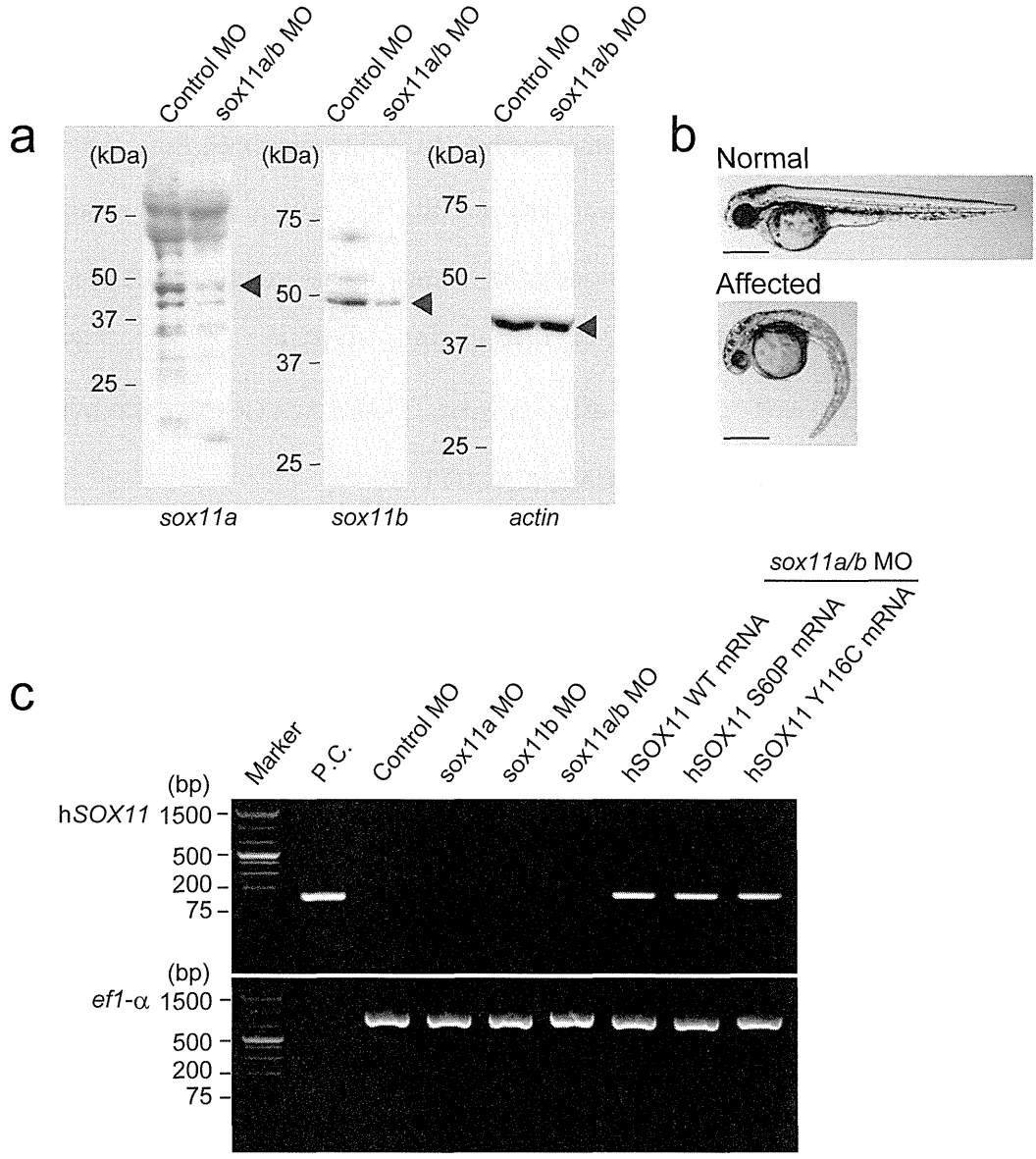

Supplementary Figure 5. *sox11* knockdown and exogenous human *SOX11* transcripts in rescue experiments.

(**a**) Efficacy of *sox11a*- and *sox11b*-MO was demonstrated by western blot analysis of *sox11a/b* loss in 48 hpf embryos, using an antibody raised against the N-terminal region of zebrafish *sox11a* (55854s, AnaSpec) (dilution 1:500) or *sox11b* (55855, AnaSpec) (dilution 1:500). Injection of a control-MO had no effect on protein levels. Actin (ab6276, Abcam) was used as a loading control. Arrowhead indicated the specific band of the detected proteins (sox11a; ~48 kDa, sox11b; ~48 kDa, actin; 42 kDa). (**b**) Gross morphology of

normal and affected embryos injected with control- and *sox11a/b*-MO. Lateral view of MO-injected embryos at 48 hpf is shown. Scale bar=500 μm. (**c**) RT-PCR using human *SOX11* (h*SOX11*) primers and zebrafish *ef1-α* on RNA extracted from positive control (P.C.) (plasmid DNA from WT h*SOX11* in the pEF6/V5-His B construct), control MO, *sox11* MO and h*SOX11* mRNA injected embryos at 24 hpf. Substantial exogenous h*SOX11* transcripts are detected in each rescue experiment. Primer sequences are hSOX11-forward: 5′-ATCGAACGCAGGAAGATCATGG-3′, hSOX11-reverse: 5′-TACTTGTAGTCGGGGTAGTCGG -3′, ef1-α-forward, 5′-ACCACCGGCCATCTGATCTACAAA-3′ and ef1-α-reverse, 5′-ACGGATGTCCTT GACAGACACGTT -3′.

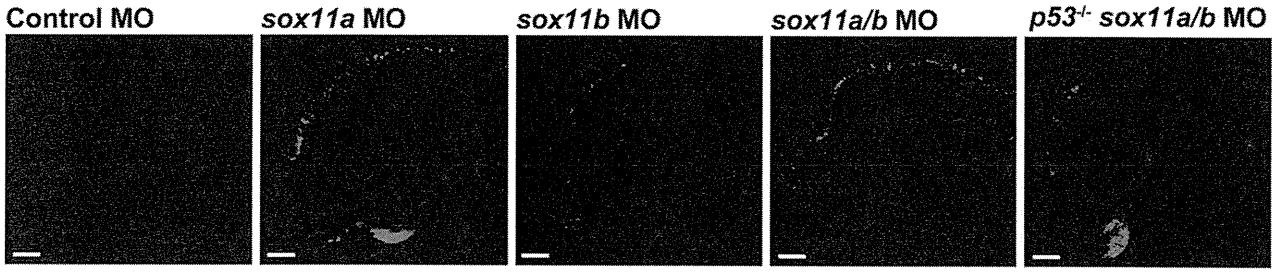

Supplementary Figure 6. Apoptotic brain cells in zebrafish with *sox11* suppression.

TUNEL staining for detection of apoptotic cells in zebrafish brain at 30 hpf. Representative examples of control-, *sox11a*-, *sox11b*-, *sox11a/b*-MO injected in WT, and *sox11a/b*-MO injected in $p53^{-/-}$ ($tp53^{zdf1/zdf1}$ mutant) embryos are shown. Obvious brain apoptosis was observed in each morphant. Scale bar=100 μm.

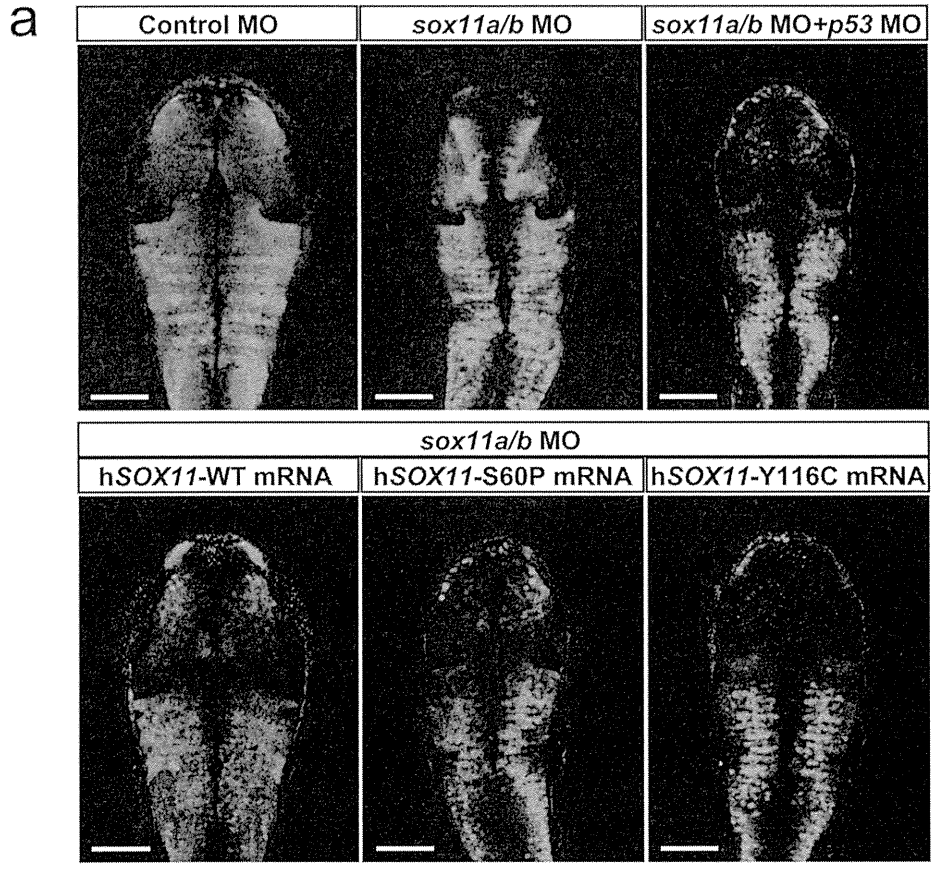
a
Control MO
sox11a/b MO
sox11a/b MO+p53 MO
sox11a/b MO
hSOX11-WT mRNA
hSOX11-S60P mRNA
hSOX11-Y116C mRNA

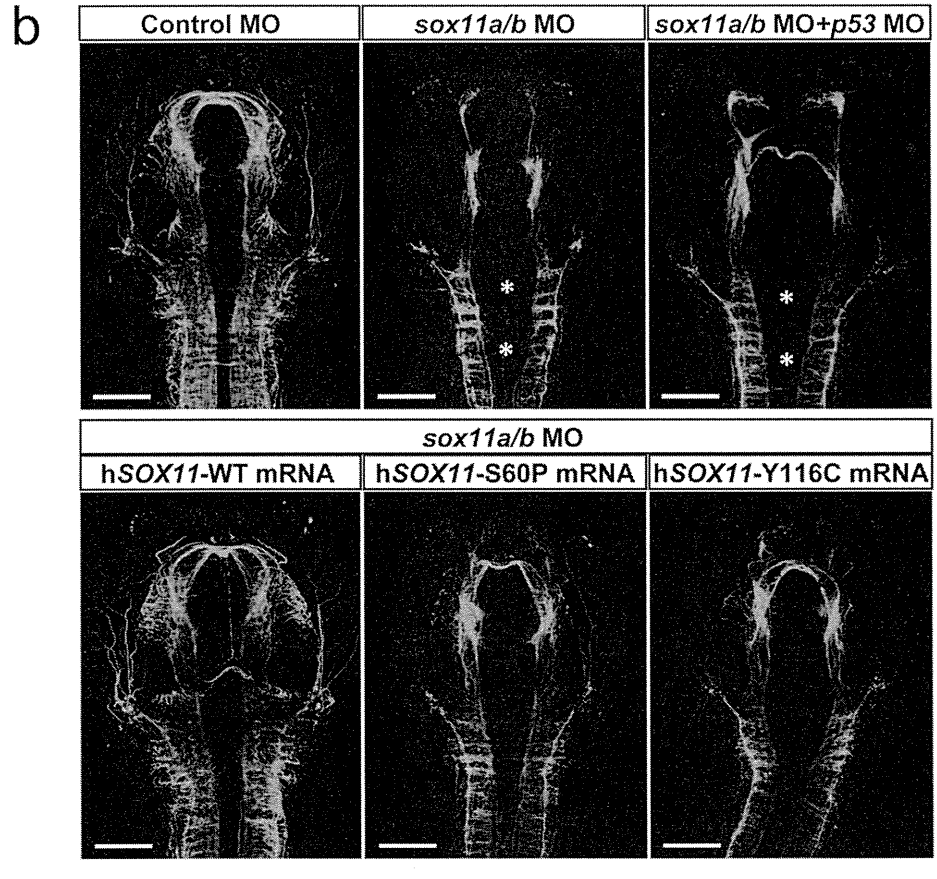
b
Control MO
sox11a/b MO
sox11a/b MO+p53 MO
sox11a/b MO
hSOX11-WT mRNA
hSOX11-S60P mRNA
hSOX11-Y116C mRNA

Supplementary Figure 7. Neuroanatomical defects in zebrafish with *sox11* suppression are rescued by human *SOX11* mRNA.

Representative dorsal views of maximum-intensity projection images following immunolabelling with anti-HuC/D (**a**) and anti-acetylated tubulin (**b**) at 48 hpf. *sox11a/b*-MO injected embryos show disorganized hindbrain commissures (asterisk). Human wild type (WT) *SOX11* overexpression more frequently restored neuroanatomical defects [HuC/D, 9/12; AcTub, 10/12 (normal/observed)], compared with S60P and Y116C mutant expression [HuC/D, S60P=1/10 and Y116C=1/11; AcTub, S60P=1/10 and Y116C=2/11 (normal/observed)]. Scale bar=100 μm.

Supplementary Table 1. Database registered *SOX11* mutations and variants

Variant	Amino acid change	rs ID	Allele frequency	Database	SIFT	PolyPhen-2	MutationTaster	Note
c.178T>C	**p.Ser60Pro**				**0 (damaging)**	**0.77 (possibly damaging)**	**1 (disease causing)**	**in this study**
c.347A>G	**p.Tyr116Cys**				**0 (damaging)**	**0.998 (probably damaging)**	**1 (disease causing)**	**in this study**
c.33G>A	p.Glu11Glu (SC)	rs369950584	0.008% (1/13003)	ESP6500				
c.49G>C	p.Glu17Gln	rs149438305	0.008% (1/13003)	ESP6500	0.04 (damaging)	0.791 (possibly damaging)	0.652 (disease causing)	
c.63G>T	p.Thr21Thr (SC)	rs139885563	0.062% (8/12996)	ESP6500				
c.318G>A	p.Arg106Arg (SC)	rs373477453	0.008% (1/13005)	ESP6500				
c.342C>G	p.Pro114Pro (SC)	rs200996693	0.046% (1/2179)	1000 Genomes				
c.345C>T	p.Asp115Asp (SC)	rs375609915	0.008% (1/13003)	ESP6500				
c.393G>A	p.Lys131Lys (SC)	rs199680382	0.046% (1/2179)	1000 Genomes				
c.401C>T	p.Ala134Val	rs374256122	0.008% (1/12825)	ESP6500	0.04 (damaging)	0.099 (benign)	0.99 (disease causing)	
c.428_433dup	p.Ala143_Gly144dup		0.087% (1/1150)	In-house 575				inframe
c.437_460del	p.Gly146_Gly153del		0.087% (1/1150)	In-house 575				inframe
c.638C>G	p.Ala213Gly		0.087% (1/1150)	In-house 575	0.3 (tolerated)	0 (benign)	0.001 (polymorphism)	
c.642C>A	p.Gly214Gly (SC)		0.087% (1/1150)	In-house 575				
c.645G>A	p.Lys215Lys (SC)	rs377652465	0.066% (8/12036)	ESP6500				
c.699_701dup	p.Asp233dup		0.1% (10/10016)	ESP6500				inframe
c.699_701del	p.Asp233del		9.42% (944/10016)	ESP6500				inframe
c.709C>G	p.Leu237Val	rs140772793	0.08% (10/12510)	ESP6500	0.16 (tolerated)	0.001 (benign)	0.413 (polymorphism)	
c.966C>A	p.His322Gln		0.087% (1/1150)	In-house 575	0.48 (tolerated)	0.001 (benign)	0.003 (polymorphism)	
c.969G>A	p.Pro323Pro (SC)	rs371115572	0.009% (1/11331)	ESP6500				
c.1051_1062del	p.Ser351_Ser354del		0.38% (31/8233)	ESP6500				inframe
c.1054G>C	p.Gly352Arg		0.087% (1/1150)	In-house 575	0.02 (damaging)	0.134 (benign)	0.005 (polymorphism)	
c.1148del	p.Gly383Alafs*39		0.53% (53/10057)	ESP6500				frameshift
c.1185G>A	p.Val395Val (SC)	rs373473887	0.037% (4/10954)	ESP6500				

SC:Synonymous change

Supplementary Table 2. Clinical features of two patients with Coffin-Siris syndrome

Clinical features		Patient 1	Patient 2
Neurodevelopment			
	developmental delay	+	+ (Mild)
	hypototnia	+	−
	microcephaly	+	+
	small cerebellum	−	N.C.
	seizures	−	−
	Dandy-Walker	−	N.C.
	abnormal corpus callosum	−	N.C.
	vision problem	+	−
	hearing loss	−	−
Ectodermal			
	absent/hypoplastic fifth finger/toenails	+	+
	hypertrichosis	+	+
	sparse scalp hair	−	+ (Mild)
	thick eyebrow	−	−
	long eyelashes	+	−
	abnormal/delayed dentition	+	−
	non-functioning/absent tear duct	−	−
Facial			
	coarse appearance	−	−
	mid facial hypoplasia	+	−
	arched eye brow	+	+
	flat nasal bridge	+	−
	broad nose	−	−
	wide mouth	−	−
	thick lips	+	−
	everted lower lip	+	+
	abnormal ears	+	+
	high palate	+	−
	cleft palate	−	−
	ptosis	+	−
	macroglossia	−	−
	short philtrum	+	−
Skeletal			
	absent/hypoplastic fifth phalanx (hand)	N.C.	+
	absent/hypoplastic fifth phalanx (foot)	N.C.	+
	clinodactyly	+	+
	short stature	+	+
	spinal anomalies	N.C.	−
	delayed bone age	N.C.	−
Gastrointestinal			
	feeding problems	±	−
	sucking problems	+	−
	intestinal anomalies	−	−
Others			
	frequent infections	−	−
	IUGR	+	+
	joint laxity	−	−
	cardiac abnormalities	−	−
	genital abnormalities	−	hypogonadotrophic hypogonadism
	inguinal hernia	−	−
	umbilical hernia	−	−
	renal abnormalities	Left small kidney	bilateral malrotated kidneys
	diaphragmatic hernia	−	−

N.C.: not confirmed.

CLINICAL GENETICS An International Journal of Genetics, Molecular and Personalized Medicine

Clin Genet 2014

Published by John Wiley & Sons Ltd
CLINICAL GENETICS
doi: 10.1111/cge.12492

Short Report

Targeted next-generation sequencing in the diagnosis of neurodevelopmental disorders

Okamoto N., Miya F., Tsunoda T., Kato M., Saitoh S., Yamasaki M., Shimizu A., Torii C., Kanemura Y., Kosaki K.. Targeted next-generation sequencing in the diagnosis of neurodevelopmental disorders. Clin Genet 2014. © John Wiley & Sons A/S. Published by John Wiley & Sons Ltd, 2014

We developed a next-generation sequencing (NGS) based mutation screening strategy for neurodevelopmental diseases. Using this system, we screened 284 genes in 40 patients. Several novel mutations were discovered. Patient 1 had a novel mutation in *ACTB*. Her dysmorphic feature was mild for Baraitser-Winter syndrome. Patient 2 had a truncating mutation of *DYRK1A*. She lacked microcephaly, which was previously assumed to be a constant feature of *DYRK1A* loss of function. Patient 3 had a novel mutation in *GABRD* gene. She showed Rett syndrome like features. Patient 4 was diagnosed with Noonan syndrome with *PTPN11* mutation. He showed complete agenesis of corpus callosum. We have discussed these novel findings.

Conflict of interest

The authors report no conflicts of interest.

N. Okamoto[a], F. Miya[b], T. Tsunoda[b], M. Kato[c], S. Saitoh[d], M. Yamasaki[e], A. Shimizu[f], C. Torii[g], Y. Kanemura[h,i] and K. Kosaki[g]

[a]Department of Medical Genetics, Osaka Medical Center and Research Institute for Maternal and Child Health, Osaka, Japan, [b]Laboratory for Medical Science Mathematics, Center for Integrative Medical Sciences, RIKEN, Yokohama, Japan, [c]Department of Pediatrics, Yamagata University Faculty of Medicine, Yamagata, Japan, [d]Department of Pediatrics and Neonatology, Nagoya City University Graduate School of Medical Sciences, Nagoya, Japan, [e]Department of Pediatric Neurosurgery, Takatsuki General Hospital, Osaka, Japan, [f]Division of Biomedical Information Analysis, Iwate Tohoku Medical Megabank Organization, Iwate Medical University, Iwate, Japan, [g]Center for Medical Genetics, Keio University School of Medicine, Tokyo, Japan, [h]Division of Regenerative Medicine, Institute for Clinical Research, Osaka National Hospital, National Hospital Organization, Osaka, Japan, and [i]Department of Neurosurgery, Osaka National Hospital, National Hospital Organization, Osaka, Japan

Key words: Baraitser-Winter syndrome – *DYRK1A* – *GABRD* – next-generation sequencing

Corresponding author: Nobuhiko Okamoto, Department of Medical Genetics, Osaka Medical Center and Research Institute for Maternal and Child Health, 840, Murodo-cho, Izumi, Osaka 594-1101, Japan.
Tel.: +81 725 56 1220;
fax: +81 725 56 5682;
e-mail: okamoto@osaka.email.ne.jp

Received 26 April 2014, revised and accepted for publication 19 August 2014

Despite many recent studies focusing on discovering the genetic basis of neurodevelopmental diseases, it is still largely unknown. We developed a next-generation sequencing (NGS) based mutation screening strategy. We screened 284 genes known or predicted to be associated with neurodevelopmental disorders with microcephaly/macrocephaly, central nervous system (CNS) anomalies and intellectual disability (ID).

Materials and methods

We studied 40 patients with neurodevelopmental disorders. They were negative for conventional cytogenetic studies and microarray analysis. With the approval of our institutional ethics committee, the patients were analyzed using this targeted sequencing. The genomic DNA of each patient was extracted from peripheral blood using extraction kit. Detail of the cell sample preparation was described in Supporting information.

Target gene sequencing

Three microgram of each sample DNA was sheared to 150–200 bp using the Covaris DNA Shearing System (Wobum, MA, USA). To capture the target exonic DNA, we used the SureSelectXT Custom capture library (Agilent, Santa Clara, CA) for 1.6 Mb of exons of neuronal gene capture. The sequence library was constructed with the SureSelect XT Target Enrichment System for Illumina Paired-End Sequencing Library kit (Agilent) according to the manufacturer's instructions. We performed DNA sequencing of either 76- or 101-bp paired-end reads using the Illumina Genome Analyzer IIx (Illumina, San Diego, CA) and HiSeq 2000 sequencer (Illumina, San Diego, CA).

Single nucleotide variation (SNV) calling

NGS reads were aligned to the Human reference genome (GRCh37/hg19). We then excluded polymerase chain reaction (PCR) duplicates, and extracted reads uniquely mapped to the reference genome that were properly paired within the insert size within mean $\pm$ 2 standard deviation (SD) of the mean. Base calling was performed in on-target regions, those regions within 100 bp upstream and downstream of the exon capture probes. SNV and insertion and deletion (indel) calling were performed using SAM TOOLS and GATK software. We excluded known variants found in database. We then narrowed the candidates to only non-synonymous, nonsense and splice site SNVs and frame shift indels. More details of method for variant calling are described in Supporting information.

NGS base-call quality check

To analyze the quality of our base-calling algorithm, we used genotypes from HapMap database (release #28, obtained from ftp://ftp.ncbi.nlm.nih.gov/hapmap/genotypes/2010-08_phaseII+III/). Sanger sequence validation of SNVs was performed using Applied Biosystems 3730xl DNA Analyzer (Life Technologies, Carlsbad, CA).

Results

To identify the causal mutation for neuronal diseases, we designed custom capture probes for the exons of 284 neuronal genes (Table S1, Supporting information). We performed targeted genes sequencing using these probes and generated 1.7 Gb of sequence on average. The average read depth of the on-target regions was 608. To check the quality of our NGS base calls, we sequenced HapMap-JPT NA18943 using the same method as the other samples, and compared our NGS calls with the released genotype of the HapMap consortium. The genotypes for 3129 locations were comparable between the two data sets. All but 16 of the 3129 genotypes were concordant between our NGS calls and the HapMap data. We validated these mismatched 16 positions using Sanger sequencing and all 16 were consistent with our NGS calls (Tables S2 and S3). On the basis of this, we estimate the false positive and false negative rate of our SNV calling to be <0.032% (<1/3129).

Clinical reports

In all patients, developmental quotient (DQ) was measured using the Kyoto Scale of Psychological Development test.

Patient 1 with *ACTB* mutation

The 3-year-old female was born at 37 weeks of gestation by normal delivery. Her developmental milestones were markedly delayed. She sat unsupported at 18 months of age. Recently, she walked with support. She spoke several meaningful words. Her DQ was 39 at 2 years of age. Physical examination identified dysmorphic features, including a flat face, arched eyebrows, narrow palpebral fissures, low-set posteriorly rotated ears and a thin upper lip. Ophthalmological investigation revealed no colobomata. Her height was 86.3 cm (−0.8 SD), and weight was 12.3 kg (mean). Her head circumference was 50 cm (+1.2 SD) at 2 years and 6 months of age. Neuroradiological investigations revealed enlarged lateral ventricles, decreased white matter volume and pachygyria dominant in the frontal lobe (Fig. 1a,b).

A novel missense was identified in *ACTB*, c.733G>A, p.G245S. She was therefore diagnosed with Baraitser-Winter syndrome (BRWS) (1).

Patient 2 with *DYRK1A* mutation

The 7-year-old female patient was born at 39 weeks of gestation by induced delivery. Her developmental milestones were severely retarded. She could not walk independently. She had no communicative language. In addition, her visual acuity was disturbed by severe amblyopia. She could see and reach objects within 30 cm. She exhibited self-injurious behavior, temper tantrums and vocal tics by vibrating her palate. She

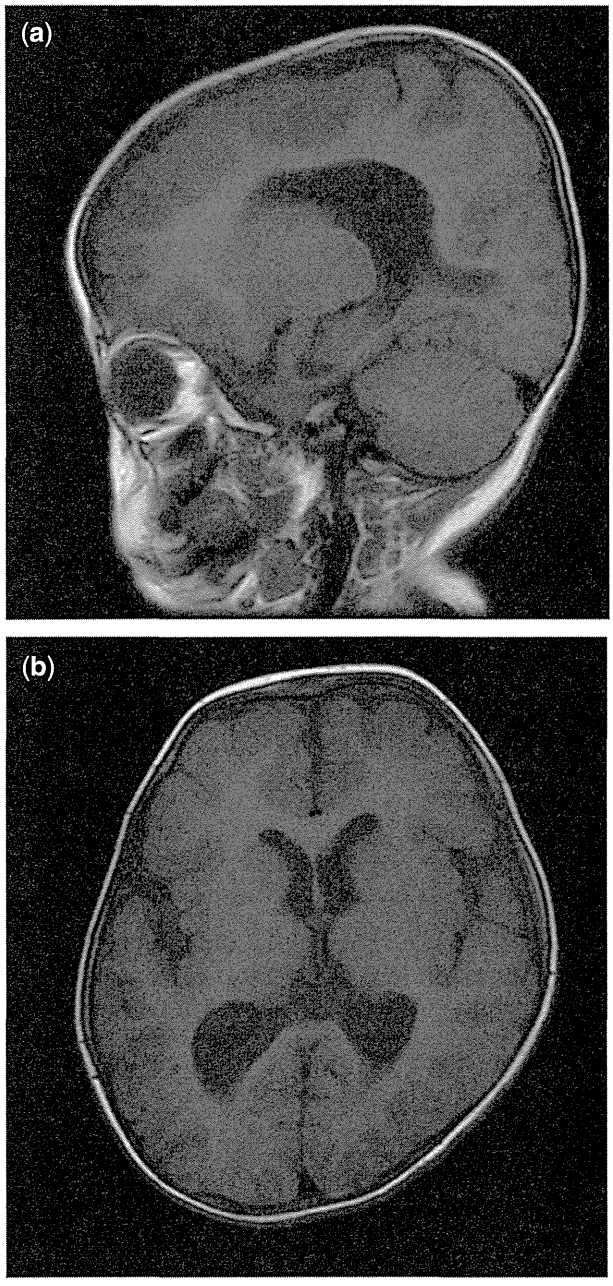

Fig. 1. (**a**, **b**) T1-weighted magnetic resonance image (MR) of patient 1 with *ACTB* mutation shows enlarged lateral ventricles, decreased white matter volume and pachygyria dominant in the frontal lobe.

was diagnosed with autism spectrum disorder (ASD) according to DSM-5. Her DQ was not properly assessed because of visual disturbance.

Physical examination identified dysmorphic features, including frontal bossing, hypertelorism, nystagmus, epicanthal folds, a flat nasal bridge, bilateral low-set ears, down-slanting palpebral fissures, a short philtrum, a high arched palate, downturned mouth and micrognathia. Her weight was 14.6 kg (−2.2 SD), height was 103.5 cm (−3.1 SD) and head circumference was 52 cm (+0.6 SD). She showed relative macrocephaly.

Brain computerized tomography (CT) and magnetic resonance imaging (MRI) were normal. Retinal abnormalities and optic nerve hypoplasia were not identified by fundoscopic investigations. Electroencephalography (EEG) showed no epileptic discharges. She had an early termination codon in exon 11 of the *DYRK1A* gene (c.C1699T: p.Q567*).

Patient 3 with *GABRD* mutation

The 12-year-old female was born at 41 weeks of gestation by induced delivery. Her development was severely retarded with generalized muscular hypotonia. She sat alone at 4 years of age. She cannot walk independently. She spoke no meaningful words. Her DQ was 12 at 9 years of age. She showed stereotyped behavior including hand gripping and bruxism. Purposeful hand skills were not obtained. She was diagnosed with Rett syndrome. EEG revealed bilateral occipital dominant high voltage slow spike and wave complex. Her height was 137 cm (−3.4 SD), weight was 35 kg (−2.1 SD) and head circumference was 51 cm (−1.8 SD). Brain CT and MRI were normal.

She had 2 bp insertion–deletion corresponding to two amino acids in *GABRD* gene (c.G498A:p.M166I and, c.G499A: p.D167N) (Fig. 2). This mutation was *de novo*.

Patient 4 with *PTPN11* mutation

The 4-year-old male was born at 40 weeks of gestation by normal delivery. Profound sensorineural hearing loss was confirmed. He was able to control his head at 4 months, roll over at 6 months of age. He could sit without support at 14 months of age. He started to walk without support at 3 years of age. His height was 90.7 cm (−1.8 SD), weight was 14.3 kg (−0.4 SD) and head circumference was 48.3 cm (−1.1 SD). Brain MRI at 4 years of age showed agenesis of corpus callosum (ACC) (Fig. 3). His DQ was 40. His dysmorphic features including hypertelorism, epicanthal folds, flat nasal bridge, low set ears, growth failure and ACC suggested the diagnosis of Mowat-Wilson syndrome. However, molecular analysis of *ZEB2* mutation was negative. Target gene sequencing revealed a heterozygous mutation in the *PTPN11* gene (c.A188G, p.Y63C). This mutation has been repeatedly reported in Noonan syndrome (NS) (2). We reevaluated his clinical features and concluded that the diagnosis of NS is appropriate. This is the first association of ACC and NS with *PTPN11* mutation.

Other patients

Three patients with cerebellar anomalies were diagnosed with mental retardation and microcephaly with pontine and cerebellar hypoplasia (MICPCH) due to *CASK* mutations. Another patient was homozygous for *AHI1* mutation. The diagnosis of Joubert syndrome was confirmed. They showed typical findings.

Discussion

ACTB mutation in patient 1 was predicted to be pathogenic in *in silico* analysis. BRWS is a rare

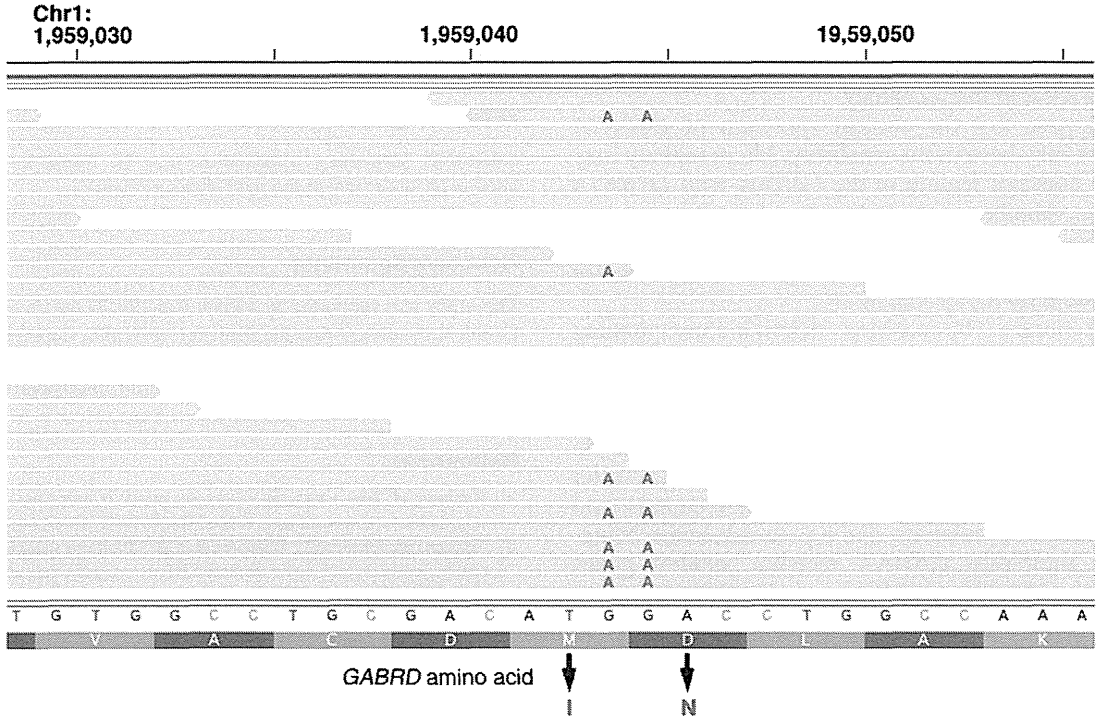

Fig. 2. Patient 3 had 2 bp insertion–deletion corresponding to two amino acids in *GABRD* gene (NM_000815: exon5: c.G498A: p.M166I and NM_000815: exon5: c.G499A: p.D167N).

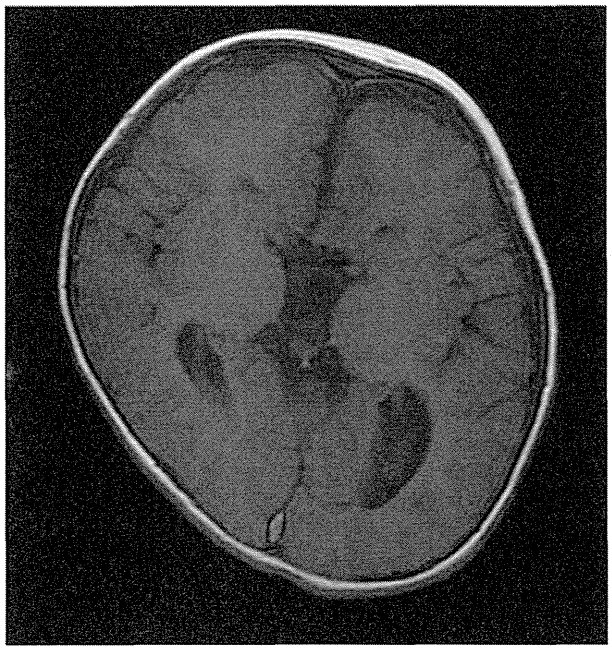

Fig. 3. Brain magnetic resonance imaging (MRI) of patient 4 with *PTPN11* mutation showed agenesis of corpus callosum

MCA/ID syndrome characterized by dysmorphic features, including ptosis, colobomata and neuronal migration anomalies (1). Rivière et al. (3) reported that mutations in *ACTB* and *ACTG1* cause BRWS. Clinical variability of BRWS is often discussed. Di Donato et al. (4) reported three patients with Fryns-Aftimos syndrome (FAS) who had a mutation in the *ACTB* gene. They suggested that mutations in *ACTB* cause a distinctly more severe phenotype than *ACTG1* mutations. They concluded that FAS is an early and severe manifestation of BRWS. Patient 1 did not show the typical features of BRWS. Her dysmorphic features were mild, and her head circumference was over average size. Recently, Verloes et al. (5) delineated the spectrum in 42 patients with BRWS. They reported that facial dysmorphism varies from mild to severe and evolves considerably over times. They suggested the designation of Baraitser-Winter cerebrofrontofacial syndrome.

Patient 2 had had severe ID, motor disturbance, autistic behavior and visual problems. She had truncating mutation of *DYRK1A*. She lacked microcephaly, which was previously assumed to be a constant feature of *DYRK1A* loss of function. *DYRK1A* is a protein kinase that belongs to the highly conserved dual-specificity tyrosine phosphorylation-regulated kinase (DYRK) family. *DYRK1A* is a highly conserved gene located in the Down syndrome critical region at 21q22. *DYRK1A* is involved in brain growth through neuronal proliferation and neurogenesis. *DYRK1A* overexpression has been implicated in ID and microcephaly in Down syndrome.

Haploinsufficiency of *DYRK1A* is associated with ID, epilepsy and microcephaly (6). So far, mutation analysis of *DYRK1A* has been carried out in patients with ID and microcephaly (7, 8). Courset et al. (9) studied the *DYRK1A* gene in a cohort of 105 patients with ID and Angelman syndrome-like symptoms, and they identified a *de novo* frameshift mutation in a patient with growth retardation, ID, and seizures. O'Roak et al. (10)

captured and sequenced 44 candidate genes in 2446 ASD probands. They discovered 27 *de novo* events in 16 genes including *DYRK1A*. The three patients with a *DYRK1A* mutation showed microcephaly.

We suppose that the clinical spectrum of *DYRK1A* mutations may have more variability. Microcephaly may not be a constant feature in the patients with *DYRK1A* mutations. Another novel finding in patient 2 was severe amblyopia. *Dyrk1A* (+/−) mice showed thin retina (11). We recommend ophthalmologic investigation for patients with *DYRK1A* mutations.

Patient 3 had a 2 bp insertion–deletion corresponding to two amino acids in *GABRD* gene. This is the first report of a *GABRD* mutation associated with Rett syndrome like features. *GABRD* encodes a subunit of the ligand-gated chloride channel for gamma-aminobutyric acid (GABA), the major inhibitory neurotransmitter (12). The majority of GABAA receptors contain two α-subunits, two β-subunits, and a γ- or δ-subunit. Mutations in inhibitory GABAA receptor subunit genes (*GABRA1*, *GABRB3*, *GABRG2* and *GABRD*) have been associated with genetic epilepsy syndromes including childhood absence epilepsy (CAE), juvenile myoclonic epilepsy (JME), pure febrile seizures (FS), generalized epilepsy with febrile seizures plus (GEFS+), and Dravet syndrome (or severe myoclonic epilepsy in infancy).

There have been some reports on the association of generalized epilepsies and *GABRD* mutations. *GABRD* gene is assigned to chromosome 1p36 (13). Patients with the 1p36 deletion syndrome often have epileptic seizures (14). Windpassinger et al. (12) found that *GABRD* is expressed most abundantly in the brain. They suggested that the *GABRD* is a good candidate for the neurodevelopmental and neuropsychiatric anomalies seen in the 1p36 deletion syndrome.

Patient 3 has been diagnosed with Rett syndrome. Heterozygous disruption of *GABRB3* produces increased epileptiform EEG activity and elevated seizure susceptibility in Angelman syndrome (15). We assume that mutant *GABRD* is likely to cause increased neuronal excitability in our patient. Further investigation is necessary to clarify mutations in Rett syndrome-like patients without known genetic causes.

Patient 4 was diagnosed with NS, the most common RASopathy characterized by short stature, distinct facial features, congenital heart defect, and ID of various degrees. Patient 4 showed ACC. So far association of NS and ACC is not known. Hypoplasia of corpus callosum is occasionally reported in cardio-facio-cutaneous syndrome, another RASopathy. We consider ACC to be an unusual manifestation of RASopathy.

Our NGS-based mutation screening strategy showed a certain success in the diagnosis of patients with neurodevelopmental disorders when conventional clinical genetic testing has proven negative. Presented patients showed unique or unexpected manifestations. We are planning whole-exome sequencing for the remaining unexplained patients.

Supporting Information

Additional supporting information may be found in the online version of this article at the publisher's web-site.

Acknowledgements

This study was supported by a grant from the Research on Applying Health Technology from the Ministry of Health, Labor and Welfare of Japan. We thank the patients and their families for participating in this work. We thank Mr K. A. Boroevich for English proofreading.

References

1. Baraitser M, Winter RM. Iris coloboma, ptosis, hypertelorism, and mental retardation: a new syndrome. J Med Genet 1988: 25: 41–43.
2. Tartaglia M, Mehler EL, Goldberg R et al. Mutations in PTPN11, encoding the protein tyrosine phosphatase SHP-2, cause Noonan syndrome. Nat Genet 2001: 29: 465–468.
3. Rivière JB, van Bon BW, Hoischen A et al. De novo mutations in the actin genes ACTB and ACTG1 cause Baraitser-Winter syndrome. Nat Genet 2012: 44: 440–444.
4. Di Donato N, Rump A, Koenig R et al. Severe forms of Baraitser-Winter syndrome are caused by ACTB mutations rather than ACTG1 mutations. Eur J Hum Genet 2014: 22: 179–183.
5. Verloes A, Di Donato N, Masliah-Planchon J et al. Baraitser-Winter cerebrofrontofacial syndrome: delineation of the spectrum in 42 cases. Eur J Hum Genet 2014 Jul 23. doi: 10.1038/ejhg.2014.95. [Epub ahead of print]
6. Moller RS, Kubart S, Hoeltzenbein M et al. Truncation of the Down syndrome candidate gene DYRK1A in two unrelated patients with microcephaly. Am J Hum Genet 2008: 82: 1165–1170.
7. Yamamoto T, Shimojima K, Nishizawa T et al. Clinical manifestations of the deletion of Down syndrome critical region including DYRK1A and KCNJ6. Am J Med Genet A 2010: 155A: 113–119.
8. Valetto A, Orsini A, Bertini V et al. Molecular cytogenetic characterization of an interstitial deletion of chromosome 21 (21q22.13q22.3) in a patient with dysmorphic features, intellectual disability and severe generalized epilepsy. Eur J Med Genet 2012: 55: 362–366.
9. Courcet JB, Faivre L, Malzac P et al. The DYRK1A gene is a cause of syndromic intellectual disability with severe microcephaly and epilepsy. J Med Genet 2012: 49: 731–736.
10. O'Roak BJ, Vives L, Fu W, Egertson JD et al. Multiplex targeted sequencing identifies recurrently mutated genes in autism spectrum disorders. Science 2012: 338: 1619–1622.
11. Laguna A, Barallobre MJ, Marchena MÁ et al. Triplication of DYRK1A causes retinal structural and functional alterations in Down syndrome. Hum Mol Genet 2013: 22: 2775–2784.
12. Windpassinger C, Kroisel PM, Wagner K et al. The human gamma-aminobutyric acid A receptor delta (GABRD) gene: molecular characterisation and tissue-specific expression. Gene 2002: 292: 25–31.
13. Emberger W, Windpassinger C, Petek E et al. Assignment of the human GABAA receptor delta-subunit gene (GABRD) to chromosome band 1p36.3 distal to marker NIB1364 by radiation hybrid mapping. Cytogenet Cell Genet 2000: 89: 281–282.
14. Rosenfeld JA, Crolla JA, Tomkins S et al. Refinement of causative genes in monosomy 1p36 through clinical and molecular cytogenetic characterization of small interstitial deletions. Am J Med Genet A 2010: 152A: 1951–1959.
15. DeLorey TM, Olsen RW. GABA and epileptogenesis: comparing gabrb3 gene-deficient mice with Angelman syndrome in man. Epilepsy Res 1999: 36: 123–132.

耳喉頭頸　87(2)：173-175，2015

原著

Waardenburg症候群2型に対する人工内耳埋め込み術後の聴覚・言語発達

大友章子　南修司郎　永井遼斗　松永達雄
榎本千江子　坂田英明　藤井正人　加我君孝

Abstract

Outcome of cochlear implantation for a girl with congenital deafness and Waardenburg syndrome tape 2

Akiko Otomo, Shujiro Minami, Ryoto Nagai, et al.
Department of Otolaryngology, National Hospital Organization Tokyo Medical Center, Tokyo, other

We reported a case of cochlear implantation in a 2 years and 2 months old girl with a left blue iris and bilateral profound hearing loss. She was diagnosed with Waardenburg syndorome type 2 by clinical findings and analysis of MITF gene mutataion demonstration. Her speech development and hearing was poor, and she underwent cochlear implantation one month later. She was educated by auditory-verbal training method after the cochlear implantation. The picture verval test shows her hearing level is getting better and is compatible with 2 years and 4months old so far.

はじめに

Waardenburg症候群は1951年にオランダの眼科医Waardenburg[1]が報告した症候群で，多くの症例は常染色体優性遺伝である。メラノサイトの発生異常が関与する色素異常症であり，皮膚白斑，前頭部白髪，虹彩異色症のほか，先天性難聴や顔貌異常，四肢異常，Hirschsprung病などをきたす[2]。1971年にArias[3]により1型，2型に分類，1983年にはKlein[4]が1型に四肢異常を伴うものを3型へと分類した。Shahら[5]はHirschsprung病を伴う例を報告し4型とした。1型と3型はPAX3，2型はSOX10やMITFなど，4型はSOX10やEDN3，EDNRBなどの遺伝子変異が原因とされている[6]。今回われわれは，臨床所見と遺伝子検査によりWaardenburg症候群2型と診断された女児に対して人工内耳埋め込み術を行い，聴覚・言語発達について経過を追ったので報告する。

症例

患者：初診時2歳2か月，現在4歳9か月の女児
主訴：両側難聴，有意語なし。
現病歴：新生児スクリーニング検査AABRで両側referとなり，目白大学耳鼻咽喉科学研究所クリニックへ紹介された。生後11日のABRで両側とも反応がなく，先天性難聴と診断された。左眼の虹彩の一部が青色であることからWaardenburg症候群が疑われ，2歳2か月で当科へ紹介された。
既往歴：特記事項なし。
家族歴：母・左先天性難聴，叔母・左眼虹彩半分が青色虹彩，叔父・右先天性難聴と左眼青色虹彩，祖父・右先天性難聴（図1）。
発達歴：定頸4か月半，寝返り10か月，座位10か月，はいはい1歳3か月，歩行1歳5か月であった。平衡バランスはやや不良で，軽度の運動発達遅滞あり，精神発達遅滞なし。
言語発達歴：4か月より補聴器装用下での教育を

受稿日：2014.11.12
おおとも　あきこ，みなみ　しゅうじろう，ながい　りょうと，えのもと　ちえこ：独立行政法人国立病院機構東京医療センター耳鼻咽喉科
まつなが　たつお，ふじい　まさと：独立行政法人国立病院機構東京医療センター臨床研究センター
かが　きみたか：独立行政法人国立病院機構東京医療センター臨床研究センター/国際医療福祉大学三田病院耳鼻咽喉科
さかた　ひであき：目白大学耳科学研究所クリニック
〔連絡先〕大友章子：独立行政法人国立病院機構東京医療センター耳鼻咽喉科（〒152-8902東京都目黒区東が丘2-5-1）